Article

Time-series of vegetation indices (VNIR/SWIR) derived from Sentinel-2 (A/B) to assess turgor pressure in kiwifruit

Alberto Jopia[1,‡,*], Francisco Zambrano[2,†,‡], Waldo Pérez-Martínez[3], Paulina Vidal-Páez[4], Julio Molina[5], Felipe de la Hoz Mardones[6]

1 Hémera Centro de Observación de la Tierra, Escuela de Agronomía, Facultad de Ciencias, Universidad Mayor, Santiago, Chile; alberto.jopia@ug.uchile.cl
2 Hémera Centro de Observación de la Tierra, Escuela de Agronomía, Facultad de Ciencias, Universidad Mayor, Santiago, Chile.; francisco.zambrano@umayor.cl
3 Hémera Centro de Observación de la Tierra, Escuela de Ingeniería Forestal, Facultad de Ciencias, Universidad Mayor, Santiago, Chile.; waldo.perez@umayor.cl
4 Hémera Centro de Observación de la Tierra, Escuela de Ingeniería Forestal, Facultad de Ciencias, Universidad Mayor, Santiago, Chile.; paulina.vidal@umayor.cl
5 Escuela de Agronomía, Facultad de Ciencias, Universidad Mayor, Santiago, Chile.; julio.molina@umayor.cl
6 Centro Especializado de Riego, Liceo Agrícola El Carmen – SNA Educa, San Fernando, Chile.; felipedelahoz@udec.cl
* Correspondence: francisco.zambrano@umayor.cl
† Current address: Updated affiliation
‡ These authors contributed equally to this work.

Simple Summary: Measures of plant water status on kiwifruit were evaluated using Sentinel-2 (A/B) for two seasons in Central Chile.

Abstract: For more than ten years, Central Chile faces drought conditions, which impact crop production and quality, increasing food security risk. Under this scenario, implementing management practices that allow increasing water use efficiency is urgent. The study was carried out in kiwifruit trees, located in the O'Higgins region, Chile; for season 2018-2019 and 2019-2020. We evaluate nine vegetation indices in the VNIR and SWIR regions derived from Sentinel-2 (A/B) satellites to know how much variability in the canopy water status could explain. Over the study's site were installed sensors that continuously measure the leaf's turgor pressure (Yara Water-Sensor). A strong correlation between turgor pressure and vegetation indices was obtained with the Spearman's rho coefficient (ρ). However, the NIR range's indices were influenced by the vegetative development of the crop rather than its water status. Red-edge showed better performance as the vegetative growth did not affect it. It is necessary to expand the study to consider higher variability in kiwifruit's water conditions and incorporate the sensitivity of different wavelengths.

Keywords: Turgor; Sentinel-2; Vegetation spectral indices; Kiwi; SWIR/NIR; time-series.

1. Introduction

In the current climate change scenario, food security and water availability are two of the main challenges facing agriculture [1]. This makes it necessary to adopt strategies that allow climate-smart agriculture and thus efficient use of water [2]. The change in precipitation patterns due to climate change in Chile has caused a prolonged drought called mega-drought [3]. Its beginning dates back

to 2007 when much of the Chilean territory was declared in agricultural emergency due to drought [4–6].The prolonged decrease in precipitation has affected the entire hydrological system in central Chile, depleting water reserves in mountains, aquifers, reservoirs, lakes and lagoons [7]. The analysis of the vegetative state in central Chile shows that during the 2019-2020 season, it is facing an extreme anomaly with respect to its normal condition (2000-2019), particularly critical for the cropland and forest land cover types [8], which is affecting the production and quality of agricultural crops. Today it is urgent to implement agricultural management practices that allow the efficient use of water to face the new water scenario.

As defined by Kirkham [9], water use efficiency (WUE) corresponds to the amount of dry matter produced for each millimeter of water that the crop uses through evapotranspiration (ET). The yield of a crop is regulated by its ET rate [10], which in terms of efficiency must be kept at a minimum optimal value that does not affect the biomass production of the crop, as below this threshold, the crop will be under stress. This threshold can be identified by measuring different components within the soil-plant-atmosphere continuum (SPAC)[11]. In the countryside, the most common practice is to measure the water potential of the leaf using the Scholander camera [12]. However, it is a destructive method that requires time and field work, which limits synoptic measurement in space. Different authors have monitored the water status of the plant focusing on the turgor pressure of the leaf [13–17], which corresponds to the pressure generated by water within the cell that compresses the plasma membrane against the cell wall [18,19]. This force decreases during the day due to the loss of water through evapotranspiration and is recovered at night. Zimmermann *et al.* [20] developed a patch clamp sensor that continuously transmits turgor variation. Specifically, this technique measures the attenuation of the clamping pressure applied externally on the sheet by the patch clamp sensor, called patch pressure (Pp)[21]. The limitation of this method is the need to have enough sensors to be able to make a spatial characterization of the turgor variation in the field.

The water status of crops can be evaluated using optical, thermal or microwave reflectance. Optical reflectance has been widely used due to water absorption characteristics in the spectral range (400–2500 nm) [22,23]. However, canopy reflectance is also influenced by factors such as the optical properties of the leaf, the geometries of observation of the sun, the reflectance of the soil, the absorption of atmospheric water and, most importantly, the way in which the leaves are organized on the tree [24–26]. Inversion of a radiative transfer model (RTM) provides one approach [22,27]; however, it requires knowledge of the parameters of the biochemical content of the leaf, which is generally time consuming. A spectral index, through the combination of reflectance at different wavelengths, has the potential to be used in regional scale applications using an empirical approach. The first applications on vegetation have been based on recovering reflectance in the visible and near infrared range (VNIR).Indices based on these regions have been used to assess the health and photosynthetic vigor of vegetation [28–31]. Examples of these are the Normalized Difference Vegetation Index (NDVI) [32] and the Enhanced Vegetation Index (EVI) [33], which incorporate the blue band into the NDVI to reduce the saturation that occurs on surfaces with high albedo values and by the dispersion of the atmosphere [33]. On the other hand, short-wave infrared reflectance (SWIR) is the most sensitive to the variation in vegetation water content due to the higher absorption coefficient [34–37]. It is typically combined with near infrared (NIR) reflectance to mitigate the impact of other factors, such as canopy structure. Some representative indices of the water status of the vegetation have been proposed. Hardisky *et al.* [38] first developed the Normalized Difference Infrared Index (NDII) to infer humidity. Gao [39] proposed the Normalized Difference Water Index (NDWI) using data from Band 2 (841–876 nm) and 5 (1230–1250 nm) from the Moderate Resolution Imaging Spectroradiometer (MODIS) to obtain vegetation water content. Fensholt and Sandholt [40] developed the Shortwave Infrared Water Stress Index (SIWSI) using MODIS band 2 (841–876 nm) and band 6 (1630–1650 nm). Xiao *et al.* [41] referred to the NDII as the SPOT-4 satellite-based land surface water index. The new multispectral sensor (MSI) attached to the Sentinel-2 (A/B) satellites provides opportunities for vegetation monitoring due to its higher spatial resolution (10/20/60 m), a spectral range of 13 bands

 doi:10.20944/preprints202009.0625.v1

from 443 to 2190 nm and a revisit capable of covering the Earth every five days [42]. Simulation studies [43] have been carried out to evaluate the usefulness of Sentinel-2 data to estimate the leaf area index (LAI) and chlorophyll, while its ability to estimate the water content of the crop it has been less investigated. The objective of this study is to evaluate the use of time series of spectral indices derived from Sentinel-2 images, obtained during the seasons 2018-2019 and 2019-2020 to detect turgor pressure in kiwifruit trees. Different vegetative indicators obtained from wavelengths in the VNIR and SWIR and their relationship with measurements of foliar turgor will be analyzed.

2. Materials and Methods

2.1. Study Area

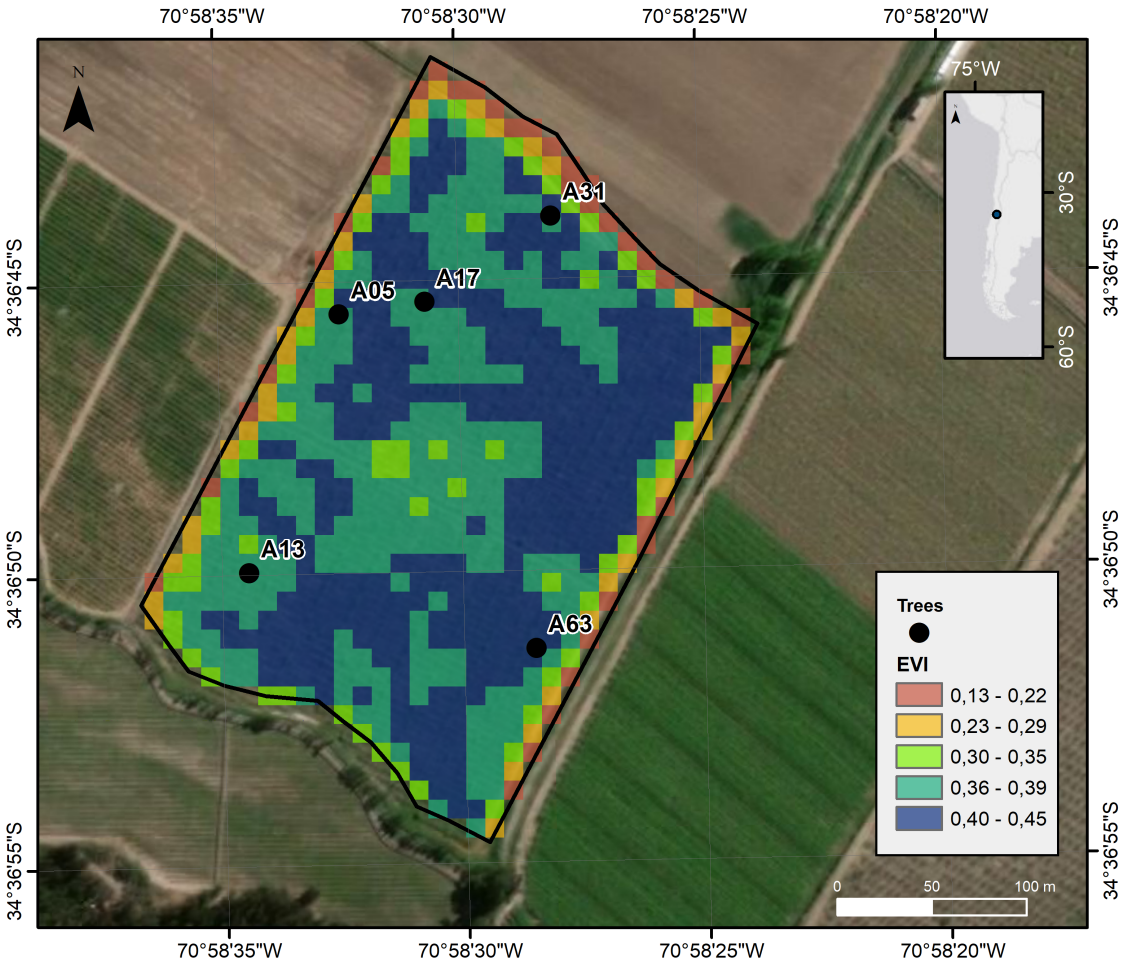

Figure 1. Study area of Kiwifruit orchard on El Carmen agricultural high school, San Fernando, Chile.

El Carmen agricultural high school is located in the commune of San Fernando, O'Higgins región, Chile (Figure 1). The species studied was kiwi (*Actinidia deliciosa*) Hayward variety, cultivated in a loamy textured soil. The orchard under study was planted in 2009 and has an area of 6.5 ha, divided into two barracks of 3 ha each with 3 irrigation subunits, with a 4.5 m x 3 m planting frame, in a conduction system of New Zealand vineyard and a localized irrigation system with 36 lt/hr micro-sprinkler. This area has a Mediterranean climate (Csb) [44] with moderate rainfall, with an annual average of 383 mm/year in the last 10 years, concentrated in winter, with a prolonged dry season of 7 to 8 months [45]. In addition, in this fruit tree, agricultural management was carried out to enhance the yield and quality of the fruit, from the four stages of the phenological development of the tree (Table 1 and Figure 2). However, irrigation was applied supplying enough water to satisfy the

Preprints (www.preprints.org) | NOT PEER-REVIEWED | Posted: 26 September 2020 doi:10.20944/preprints202009.0625.v1

water demand of the crops, which was monitored by crop evapotranspiration [46], recovered from a meteorological station located 700 meters from the orchard. The irrigation supply had variations mainly focused on enhancing the development of the fruit. During E1 and E2 a greater and more frequent amount was applied than in E3 and E4. In these last stages, irrigation events were applied less frequently and with a longer duration to avoid the development of new foliage that would compete for nutrients with the development and maturation of the fruit [47]. The application of the water supply in each season can be observed by recording the soil moisture at different depths using a Sentek probe installed in the orchard (Figure 2).

Table 1. Description and approximate start dates of the main stages of agricultural management of Kiwi var. Hayward. Source: Modified from Sabaini and Goecke [47], Sabaini [48].

Management stage	Start	End	Description
E1: Load regulation	September 15	November 15	It begins about 10 days before budding with the start of floral differentiation. Flower buds develop until flowering. Pruning and thinning work is carried out
E2: Pollination	November 15	January 7	It begins with the pollination of the flower. The fruit develops and grows at high rates reaching 50% of its weight and 70% of its final volume. In this stage the vegetation reaches its highest water demand and the temperature reaches its maximum
E3: Vegetation management	January 7	March 15	Green pruning is carried out, corresponding to the removal of shoots and foliage in order to improve the distribution and penetration of light in the crown
E4: Fruit harvest	March 15	April 15	The maturity and harvest of fruit is ensured, it is the shortest stage and extends from the third week of March to mid-April.

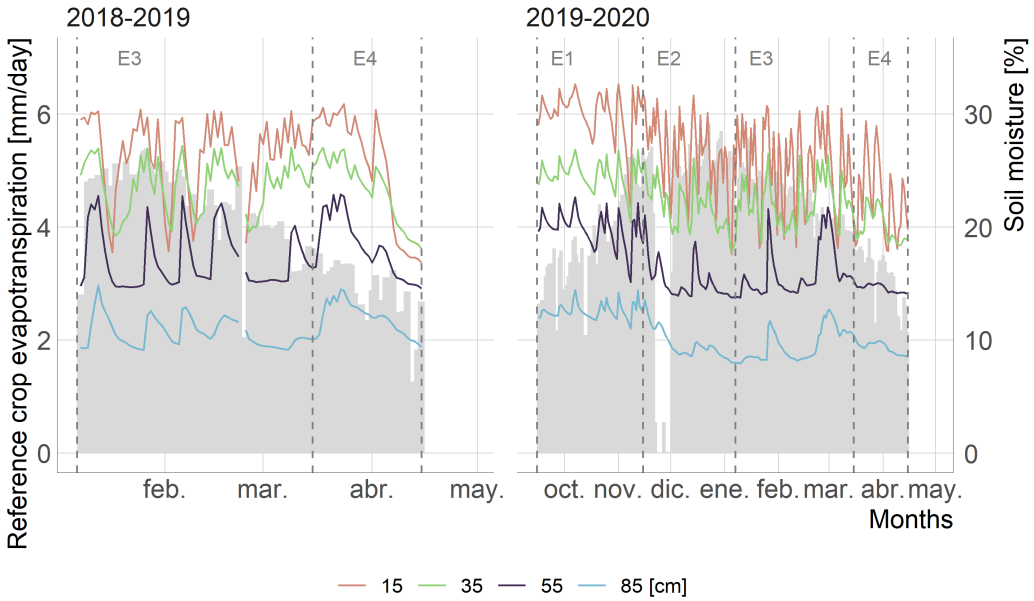

Figure 2. Variation of crop evapotranspiration and soil moisture content at different depths (15, 35, 55 and 85 cm) in the kiwi orchard for the 2018-2019 and 2019-2020 season. Horizontal lines correspond to the depths of soil moisture of the Sentek probe.

Preprints (www.preprints.org) | NOT PEER-REVIEWED | Posted: 26 September 2020 doi:10.20944/preprints202009.0625.v1

2.2. Data

2.2.1. Sentinel-2

The Sentinel-2 mission of the European Space Agency (ESA) is composed of two twin satellites, A and B, which have a multispectral sensor with 13 spectral bands at a spatial resolution of 10, 20 and 60 m depending on the spectral region (Table 2). Each satellite has a time frequency of five days. In this study, 52 images captured between February 5, 2019 and April 11, 2020 were used. The images were downloaded and atmospherically corrected at L2A level (Bottom of the Atmosphere; BOA) with the sen2r package [49] in the R software [50].

Table 2. Spectral bands of the Sentinel-2 mission. The central wavelength corresponds to the sensors on the Sentinel-2 satellites A and B. Source: Adapted from ESA [42]

Bands	Spatial Resolution (m)	Central wavelength (μm) (A;B)
B1 - Coastal aerosol	60	442.7; 442.2
B2 - Blue	10	492.4; 492.1*
B3 - Green	10	559.8; 559.0*
B4 - Red	10	664.6; 664.9*
B5 - Red Edge	20	704.1; 703.8*
B6 - Red Edge	20	740.5; 739.1
B7 - Red Edge	20	782.8; 779.7
B8 - NIR	10	832.8; 832.9*
B8A - Red Edge	20	864.7; 864.0
B9 - Water vapour	60	945.1; 943.2*
B10 - SWIR - Cirrus	60	1373.5; 1376.9
B11 - SWIR	20	1613.7; 1610.4*
B12 - SWIR	20	2202.4; 2185.7*

Note: * band used in the study

2.3. Patch pressure (Pp) Yara Water-Sensor

The continuous monitoring of the vegetation water status was based on the technique developed by Zimmermann *et al*. [20], who, using a pressure sensor, recovered the changes in the turgor of the leaf. This technique measures the pressure transfer function of a leaf, called patch pressure (Pp), which corresponds to the variation in the clamping pressure of the sensor as a result of the counter force exerted by the leaf tissue. The Pp is inverse to the turgor pressure, so that the increase in the magnitudes of Pp implies low values of leaf turgor and shows a decrease in the water status of the plant [15].

The turgor pressure sensors (Yara Water-Sensor) were used, made up of two imanes that were fastened to the plant leaf as indicated in Figure 3. One face had a rectangular cutout that housed a pressure microsensor, which automatically and continuously transmitted a reading every five minutes to a web server, without affecting the development of the plant. To monitor the water status of the vegetation, Yara Water-Sensors were installed in five kiwi trees (Table 3), in which the Pp was measured. These sensors were attached to two or three leaves of each tree, which presented similar characteristics (size, color, state of growth). The Pp measurements were made for the 2018 season, between February 5 to May 15, 2019; and for the 2019 season, between October 12, 2019 to April 11, 2020.

Table 3. Yara Water-Sensors installed in each monitored tree.

Tree	Number of Yara Water-Sensors 2018-2019	2019-2020
A05	2	2
A13	2	2
A17	3	1
A31	2	2
A63	2	2

Preprints (www.preprints.org) | NOT PEER-REVIEWED | Posted: 26 September 2020 doi:10.20944/preprints202009.0625.v1

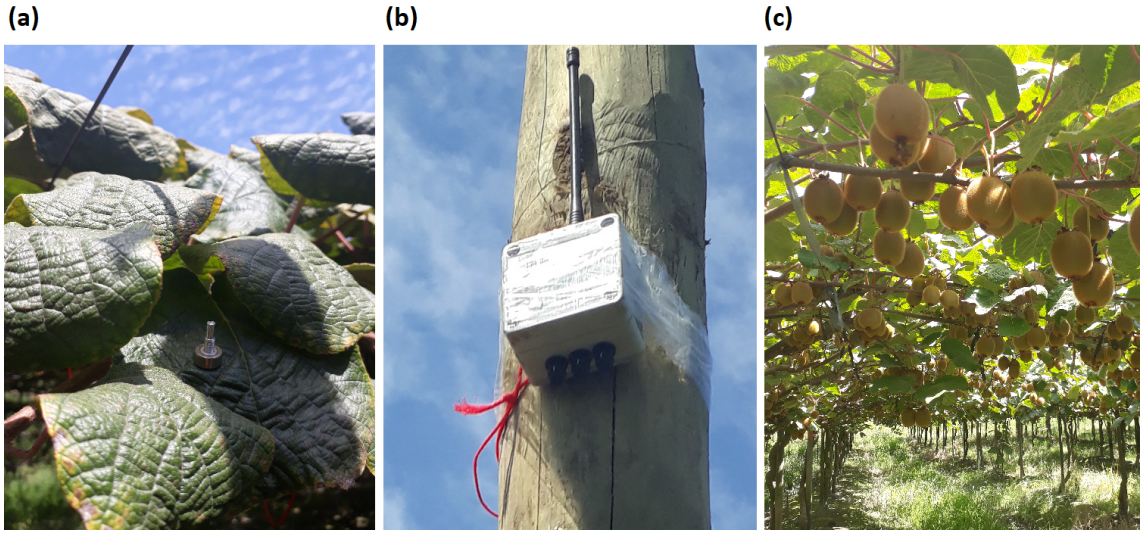

Figure 3. (**a**) Yara Water-Sensors installed in the field. (**b**) Transmitter that receives the signal from the Yara Water-Sensors installed on each leaf of the tree. (**c**) foliage of the kiwi crop.

2.4. Spectrals vegetation indices

Nine vegetation indices based on the VNIR and SWIR spectral range derived from the Sentinel-2 satellite were used. Table 4 presents the vegetation indices, among which the enhanced vegetation index (EVI) and the normalized difference infrared index (NDII) highlight. This last indicator is found in the literature under various names, associated with a spectral variation in the SWIR and the sensor used. [36] reviewed and determined the names of NDWI, NDII, and NBR for SWIR lengths of (1) 1–1.3 μm, (2) 1.55–1.75 μm, and (3) 2.05–2.45 μm, respectively.

Table 4. Evaluated spectrals vegetation indices derived from Sentinel-2.

Wavelength	Vegetation Index	Formula	Reference
VNIR	Enhanced Vegetation Index (EVI)	$\frac{2.5(B8-B4)}{((B8+6B4-7.5B2)+1)}$	[33]
VNIR	Red edge 1 (Rededge1)	$\frac{B5}{B4}$	[51]
VNIR	Leaf Chlorophyll Index (LCI)	$\frac{(B8-B5)}{(B8+B4)}$	[52]
VNIR	Normalized Difference Vegetation Index (NDVI)	$\frac{(B8-B4)}{(B8+B4)}$	[32]
VNIR	Chlorophyll Absorption Ratio Index (CARI)	$\frac{B5}{B4}\frac{\sqrt{(\frac{B5-B3}{150}670+B4+(B3-(\frac{B5-B3}{150^2}550)))^2}}{(\frac{B5-B3}{150^2+1})^{0}.5}$	[53]
VNIR-SWIR	Normalized Difference Infrared Index (NDII)	$\frac{(B8-B11)}{(B8+B11)}$	[38]
VNIR-SWIR	Normalized burn ratio Index (NBR)	$\frac{(B9-B12)}{(B9+B12)}$	[54]
VNIR-SWIR	Global Vegetation Moisture Index (GVMI)	$\frac{((B9+0.1)-(B12+0.02))}{((B9+0.1)+(B12+0.02))}$	[55]
VNIR-SWIR	Simple Ratio MIR/NIR Ratio Drought Index (RDI)	$\frac{B12}{B9}$	[56]

Vegetation indices were calculated for the 52 available dates. Then, the values of the indices for each tree were extracted. In order to eliminate data with clouds; the dates of the winter and autumn months were removed with NDVI values lower than 0.2, threshold corresponding to the minimum value that the kiwi crop reached in those months. In Figure 4 the 44 dates selected for the CARI index are presented.

Preprints (www.preprints.org) | NOT PEER-REVIEWED | Posted: 26 September 2020 doi:10.20944/preprints202009.0625.v1

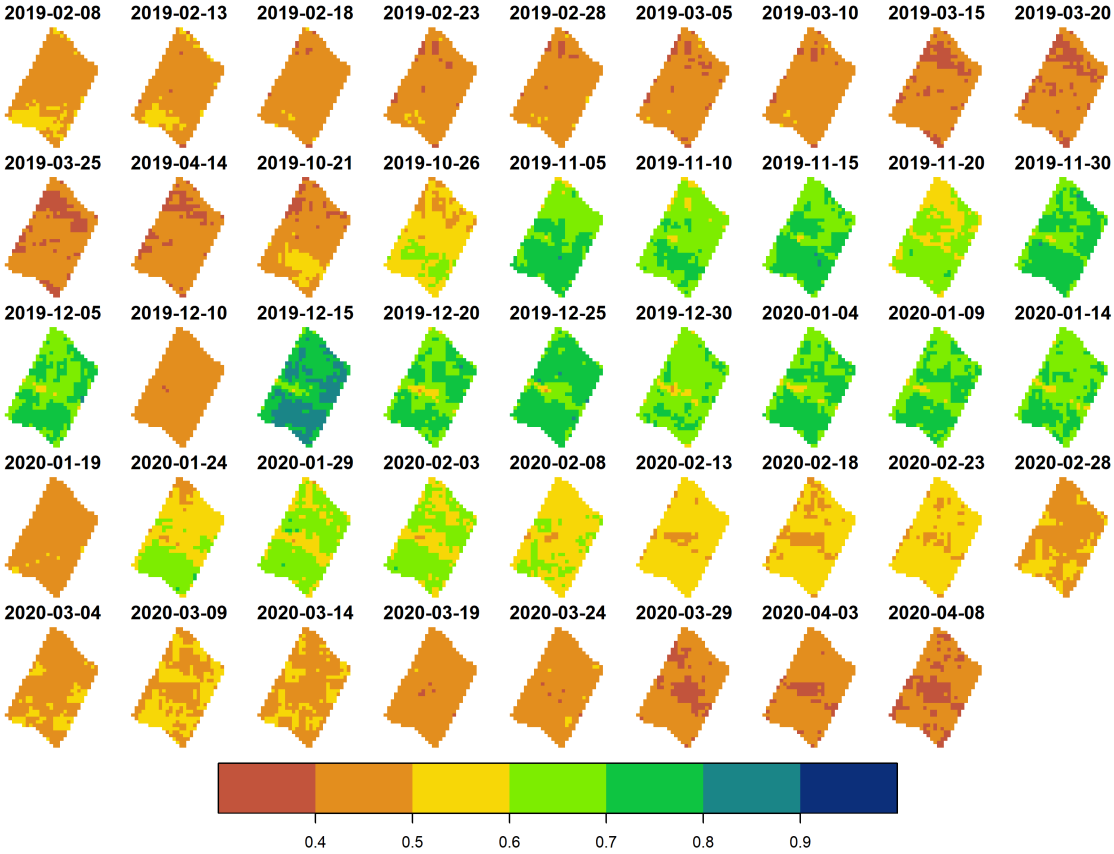

Figure 4. CARI time series for selected dates.

2.5. Exploratory analysis

The Pp data obtained from the different Yara Water-sensors for the 2018-2019 and 2019-2020 seasons were subjected to a cleaning procedure to remove anomalous data. The data from the Water Yara sensors that had a record lower than 30% were eliminated, and also those records that had at least 3 periods with discontinuities and oscillation of their magnitude of at least 100%. Then, outliers were eliminated for a weekly period, defining a range between the weekly average $\pm$ two standard deviations. In addition, the monthly outliers were removed by narrowing a range between the monthly average $\pm$ two standard deviations.

Subsequently, the Pp records were summarized daily according to the Sentinel-2 revisit time interval, by calculating the average of Pp every 15 minutes between 15:00 - 16:00 UTC, since Sentinel-2 passes over Chilean territory at ~15:30 UTC. Because between the 2018-2019 and 2019-2020 seasons the kiwi trees lose their leaves, the sensors had to be reinstalled on new leaves from the same tree. Thus, to avoid errors associated with sensor installation, the pressure measurements were considered independent of each other and only the variation of each sensor in each season was considered, which was determined by applying a standardization through the average and standard (Equation 1)[57].

$$z_i = \frac{x_i - \bar{x}}{\sigma} \tag{1}$$

Where z_i value is the standardized value of x_i; an element of a data sample with mean $\bar{x}$ and standard deviation σ.

Regarding the analysis of the vegetation indices, those that presented the lowest correlation between them were selected to avoid redundancy. The selection was based on a correlation matrix based on Pearson's coefficient [58]. Experimentally, the average correlation threshold was determined for each index of $r \leq 0.7$ and $r \leq 0.97$, for indices based on VNIR and VNIR-SWIR, respectively. In

Preprints (www.preprints.org) | NOT PEER-REVIEWED | Posted: 26 September 2020 doi:10.20944/preprints202009.0625.v1

order for the vegetation indices to be comparable with the Pp measurements, the values of each season were standardized with Equation 1.

2.6. Correlation analysis

To relate the Pp measurements with the Spectral indices, the average value of the values in the existing Pp sensors in each tree was used (Table 3). The association of vegetation indices with temporal changes in Pp was evaluated using Pearson's coefficient (r) [58] and Spearman's non-parametric coefficient rho (ρ) [59]. Additionally, the relationship between both variables was evaluated using a linear regression model, obtaining the metrics of the root mean square error (RMSE) and the coefficient of determination (r^2) [60,61].

3. Results

3.1. Exploratory analysis

The analysis of the correlation matrix for the vegetation indices (Figure 5) determined that there was a high relationship between the indices constructed with spectral bands at the VNIR-SWIR wavelength, specifically with an r between [0.94 - 1]. Greater variability was obtained between the indices belonging to the VNIR range with values of r between [0 - 0.99]. The CARI index stood out for presenting the greatest heterogeneity, which would be explained by the spectral behavior of the green band that is not found in the other indices. The indicators with the lowest correlation that represent the VNIR and VNIR-SWIR spectral range were selected, corresponding to the CARI, EVI, Rededge1, NDII and GVM1 indices, with average r values of 0.17, 0.70, 0.70, 0.96 and 0.97, respectively.

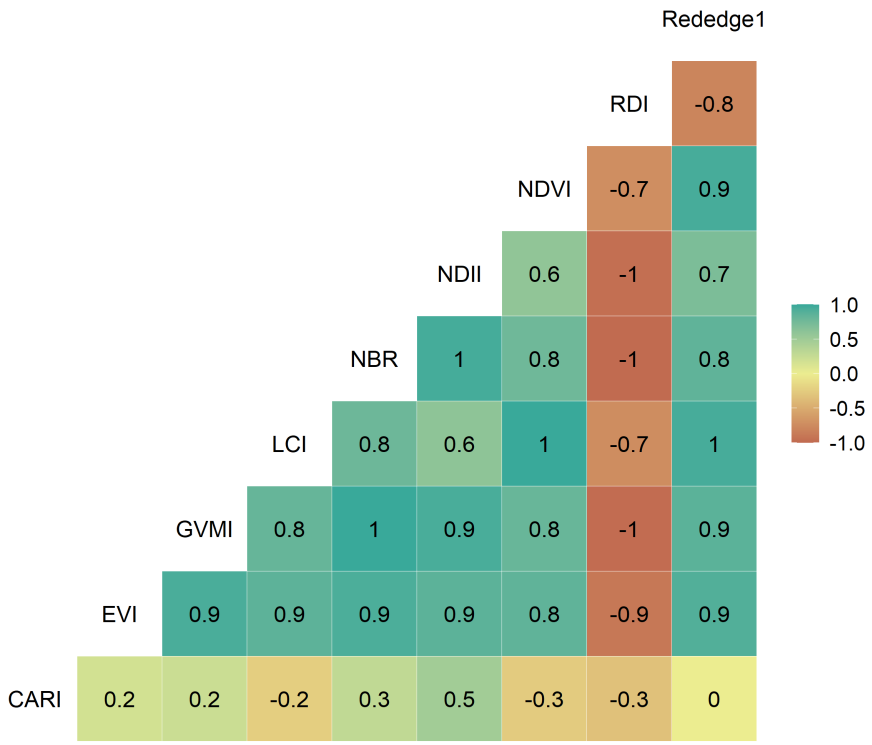

Figure 5. Correlation matrix between vegetation indices, value corresponds to Pearson's correlation coefficient (r).

Preprints (www.preprints.org) | NOT PEER-REVIEWED | Posted: 26 September 2020 doi:10.20944/preprints202009.0625.v1

Figure 6b shows the temporal variation of the vegetation indices between each stage of agricultural management (E1, E2, E3 and E4) for each tree. The trend of the vegetation indices in both seasons is in accordance with the phenology and crop management (Figure 2), since the magnitudes of the indices begin to increase from E1 until reaching the maximum photosynthetic vigor in E2, and from E3 the values in both seasons have a decreasing trend. The spatial variability of the vegetation indices was low, reaching a maximum standard deviation of 0.13, except for CARI, which reached values of 0.43 in the 2018-2019 season. Figure 4 shows the CARI spatio-temporal series where the spatial variability achieved in the orchard is represented.

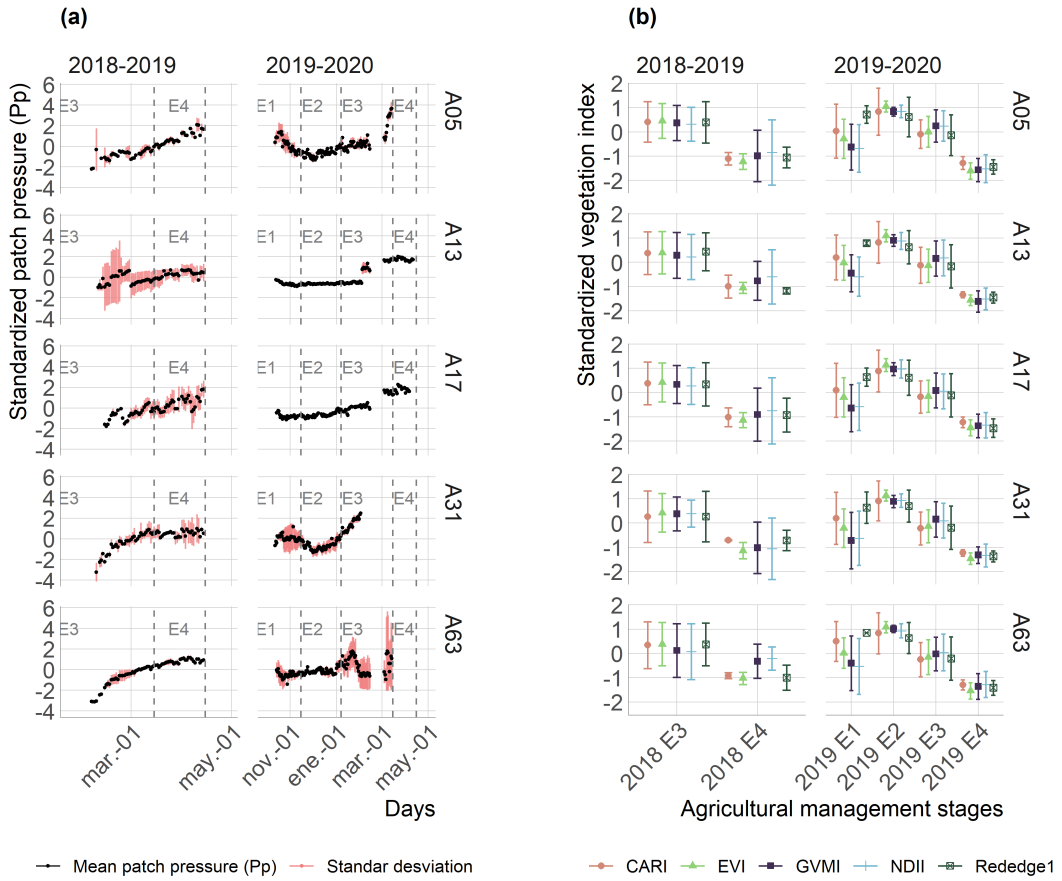

Figure 6. (**a**) Average patch pressure (Pp) for each tree (black line) and its standard deviation (red line). (**b**) values of the vegetation indices for each tree grouped for each stage of agricultural management through the average and standard deviation.

Regarding the Pp sensors (Figure 6a), the temporal dynamics presents a differentiated behavior between the stages of agricultural management. In E1 and E2, season 2019-2020, the Pp begins with a decrease in its magnitude and then maintains its values, showing a stable behavior over time, which indicates the maintenance of the hydric state of the leaf. On the other hand, in E3 and E4 there is an increase in the magnitudes of Pp, evidenced by the loss of leaf turgor, which is related to a decrease in its hydric state. However, the lack of data on trees for the 2019-2020 season and the variability between sensors limits the reliability of the analysis.

The variability obtained between the sensors of each tree (Figure 6a and Table 5) indicates that it is higher in E3 and E4, with values in the range [0.41, 0.63], followed by E1 and E2, with values of 0.36 and 0.23, respectively. This behavior is related to a differentiated effect of the leaves due to agricultural management, as in the stages where there was greater variability, destructive procedures

Preprints (www.preprints.org) | NOT PEER-REVIEWED | Posted: 26 September 2020 doi:10.20944/preprints202009.0625.v1

were carried out on the plant. Specifically, foliage removal tasks were carried out in E1 and E3, and the fruit was harvested in E4. On the contrary, E2 had a non-destructive management corresponding to flower pollination and fruit growth and development (Table 1).

Table 5. Average of the standard deviation obtained from Pp in each tree and stage for the 2018-2019 and 2019-2020 seasons.

	2018-2019		2019-2020			
Tree	**E3**	**E4**	**E1**	**E2**	**E3**	**E4**
A05	0.42	0.25	0.56	0.14	0.31	-
A13	1.34	0.64	0.11	0.04	0.12	0.05
A17	0.38	0.90	-	-	-	-
A31	0.40	0.54	0.89	0.42	0.31	-
A63	0.30	0.14	0.51	0.22	1.43	-
Mean	**0.54**	**0.49**	**0.52**	**0.20**	**0.54**	**0.05**

3.2. Correlation analysis

The linear regression model used for the Pp and the vegetation indices presented biases in the residuals; therefore, the results of the Pearson correlation coefficient were not included in the analysis and only the Spearman ρ coefficient and the root mean square error (RMSE). Spearman's analysis for the temporal dynamics of Pp and the vegetation indices (Figure 7a) of the 2018-2019 season presented a strong relationship in most of the trees, with EVI and GVMI being the indices that obtained the greatest association with an average value of ρ equal to -0.88 and -0.81, respectively. CARI, NDII and RedEdge1 reached an average magnitude of ρ equal to -0.77, 0.76 and 0.74 (Figure 7a). Then, in the second season, the magnitude of the association decreased for all the indices, resulting in a ρ equal to -0.65, -0.66, -0.55 and -0.44 for Rededge1, EVI, CARI and NDII, respectively. The results indicate that in the 2019-2020 season there was a lower relationship between the Pp and the vegetation indices composed of NIR, based on the behavior in E1 and E2, where the vegetation indices, with the exception of Rededge1, showed an increase of magnitude, while Pp values tended to be constant (Figure 8). It should be noted that the trees that presented the greatest variation between their Yara Water-sensors, A13 and A63 for the 2018-2019 and 2019-2020 seasons, respectively, did not have a significant relationship with the vegetation indices. Figure 7b shows the low Pp prediction capacity of the vegetation indices using a linear model, with an average value of RMSE greater than 0.5 for most of the indices of the first season and greater than 0.7 for the indices of the second season. This indicates an important error in the estimation of Pp, considering that the magnitudes of Pp on average oscillate between -1 and 2.

The performance of NDII and GMVI was expected to be higher, as unlike the other indicators, these are composed of a band in SWIR, which is sensitive to the water content of the vegetation. To improve understanding of this result, Figure 9a shows the time series of the reflectivity of the spectral bands used in the vegetation indices. The reflectivity in red obtained a slight increase from E3, while in SWIR (1610 and 2190 *nm*) and in Red edge (704 *nm*) had low variability, evidencing the lower sensitivity to changes in vegetation. In Figure 9b the average spectral signature of the five kiwi trees is shown for dates at each stage of development (E1-E4). It can be observed that the spectral region that is sensitive to the development of vegetation is in the spectral range 740-1610 *nm*, corresponding to spectral regions that are not absorbed by healthy vegetation; while regions that are highly absorbed, 442-740 *nm* and 1610-2202 *nm*, remain with a low variation. Figures 9a and 9b indicate that the reflectivity of the vegetation in NIR obtained the highest sensitivity by detecting the phenological behavior of the crop. The behavior of most vegetation indices is mainly explained by NIR.

4. Discussion

Due to the fact that the irrigation supplied was regularly homogeneous and was applied to satisfy the water demand of the crop, the changes in Pp would be explained mainly by the variation in the hydric state of the leaf driven by a synergistic effect between agricultural management, crop phenology

Preprints (www.preprints.org) | NOT PEER-REVIEWED | Posted: 26 September 2020 doi:10.20944/preprints202009.0625.v1

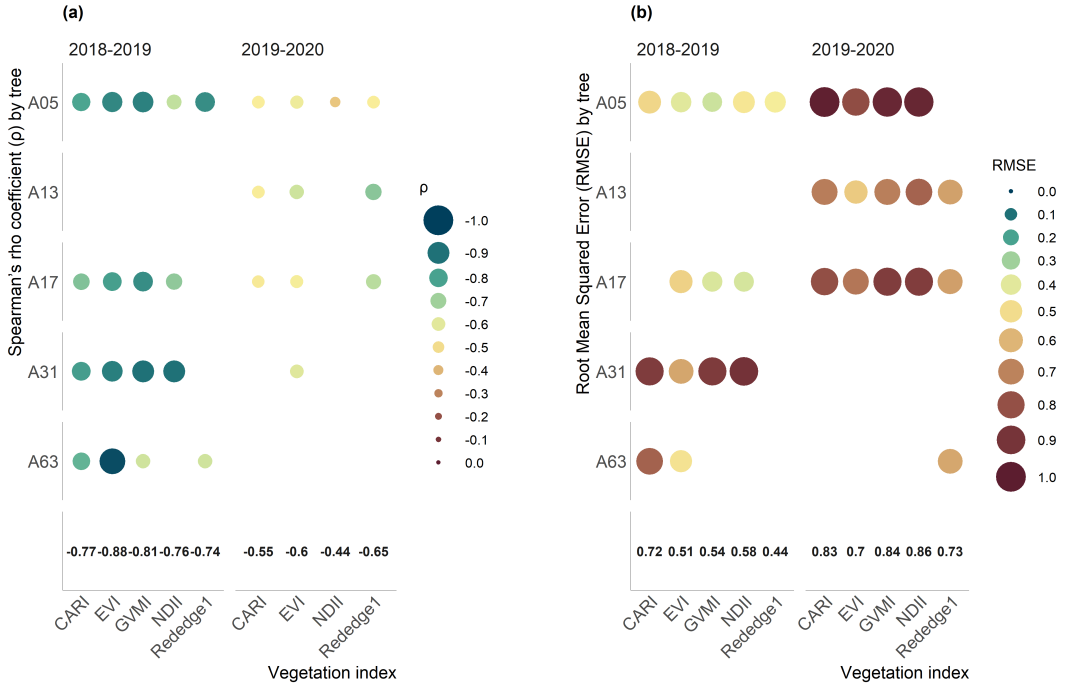

Figure 7. (**a**) Spearman's rho correlation coefficient (ρ) between Pp and vegetation indices. (**b**) Root mean squared error (RMSE) between Pp and the linear fit of each vegetation index. Both statistical analyzes have a significance of ρ <0.05. The numbers in bold correspond to the average values of ρ for each index.

and atmospheric demand. Starting at the generation of the fruit, from pollination (E2), the phloem is mobilized from the reserves of the leaves towards the fruit, gradually causing a decrease in leaf turgor [62]. This process is coupled with the greater water losses with the green pruning performed in E3, which reduces the efficiency of the leaf to retain water and not gave it to atmospheric demand. Finally, the decline in turgor pressure worsens in mid-E4 with the arrival of leaf senescence that generates a decrease in chlorophyll and recycling of foliar nutrients, followed by leaf dehydration [62].

The spectral signature of the kiwi crop shown in Figure 9b, indicates that during the four stages of agricultural management the vegetation maintains a high absorbance in the visible and SWIR lengths, evidencing the behavior of healthy and well-watered vegetation [63], being consistent with the irrigation supply. In this way, it is inferred that wavelengths that kept their reflectivity level constant are more suitable for monitoring vegetation hydric status, being these visible (442-665 *nm*), red edge (704 *nm*) and SWIR (1610 and 2190 *nm*). The Rededge1 index presented the best relationship with Pp in E1-E2, showing a low sensitivity with phenology, specifically with vegetative development, indicating that it is more suitable for monitoring the water status of the vegetation based on the turgor of the leaf. However, as the irrigation supply was applied to satisfy the atmospheric demand, the vegetation did not experience water stress. Therefore, it is necessary to include different irrigation treatments to improve the evaluation of the visible spectral ranges (442-665 *nm*), red edge (704 *nm*) and SWIR (1610 and 2190), in order to detect surplus or stress situations in the vegetation and contribute to the development of applications to improve the irrigation strategy of crops.

The vegetation indices made up of NIR showed a close relationship with the vegetative growth of the crop. The lower relationship obtained between Pp and the vegetation indices in the 2019-2020 season compared to the 2018-2019 season, indicates that the relationship between Pp and the vegetation indices composed of NIR is based on the vegetative development of the crop and it is not related to the hydric changes of the crop driven by phenology and agricultural management. This finding was

Preprints (www.preprints.org) | NOT PEER-REVIEWED | Posted: 26 September 2020 doi:10.20944/preprints202009.0625.v1

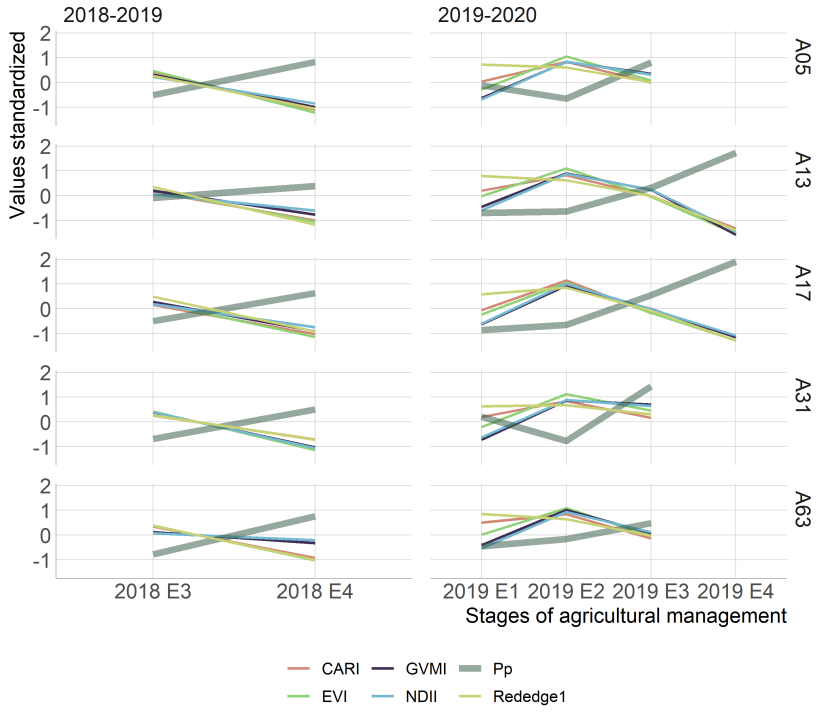

Figure 8. Temporal relationship between patch pressure (Pp) and vegetation indices. Average magnitudes per stage are shown.

reported by [64] who analyzed the relationship between the reflectance of different spectral ranges and a set of data from temperate and boreal forests of North America. These authors determined that the bands that have the greatest sensitivity with the phenology of the vegetation correspond precisely to the regions that are not used in the photosynthesis process. These are the infrared regions, which is explained by the high correlation obtained between the concentration of canopy nitrogen and the reflectance in the NIR region (800-1400 nm), compared to the low reflectance ratio in the visible region. Further studies should focus on indices that are not sensitive to vegetative development and should relate directly to the vegetation hydric status. In addition to SWIR, spectral bands in the microwave range [65,66] and thermal [35,67–70] have shown to have the qualities to identify variations in surface water content.

It was evidenced that Pp, a variable used as a predictor of the hydric status of the vegetation, is influenced by the agricultural management and phenology of the vegetation. Thus, the analysis should consider irrigation treatments that isolate this response to assess Pp changes driven by the water supply. Finally, in this study, the standardization of Pp was used as a method to remove its magnitude and mainly evaluate its temporal variability. In this way, errors associated with the installation of Yara Water-sensors between different seasons were reduced, which was of great help to represent the behavior of a tree. However, a better analysis of Pp for irrigation applications should include the magnitude to determine Pp ranges that are related to periods of water stress or surplus in the vegetation.

5. Conclusion

The Yara Water-sensor patch pressure was used as an indicator of leaf turgor to monitor the water status of five kiwi trees. The following conclusions were obtained for the irrigation regimes to which the kiwi orchard was subjected, which did not consider water restriction:

Preprints (www.preprints.org) | NOT PEER-REVIEWED | Posted: 26 September 2020 doi:10.20944/preprints202009.0625.v1

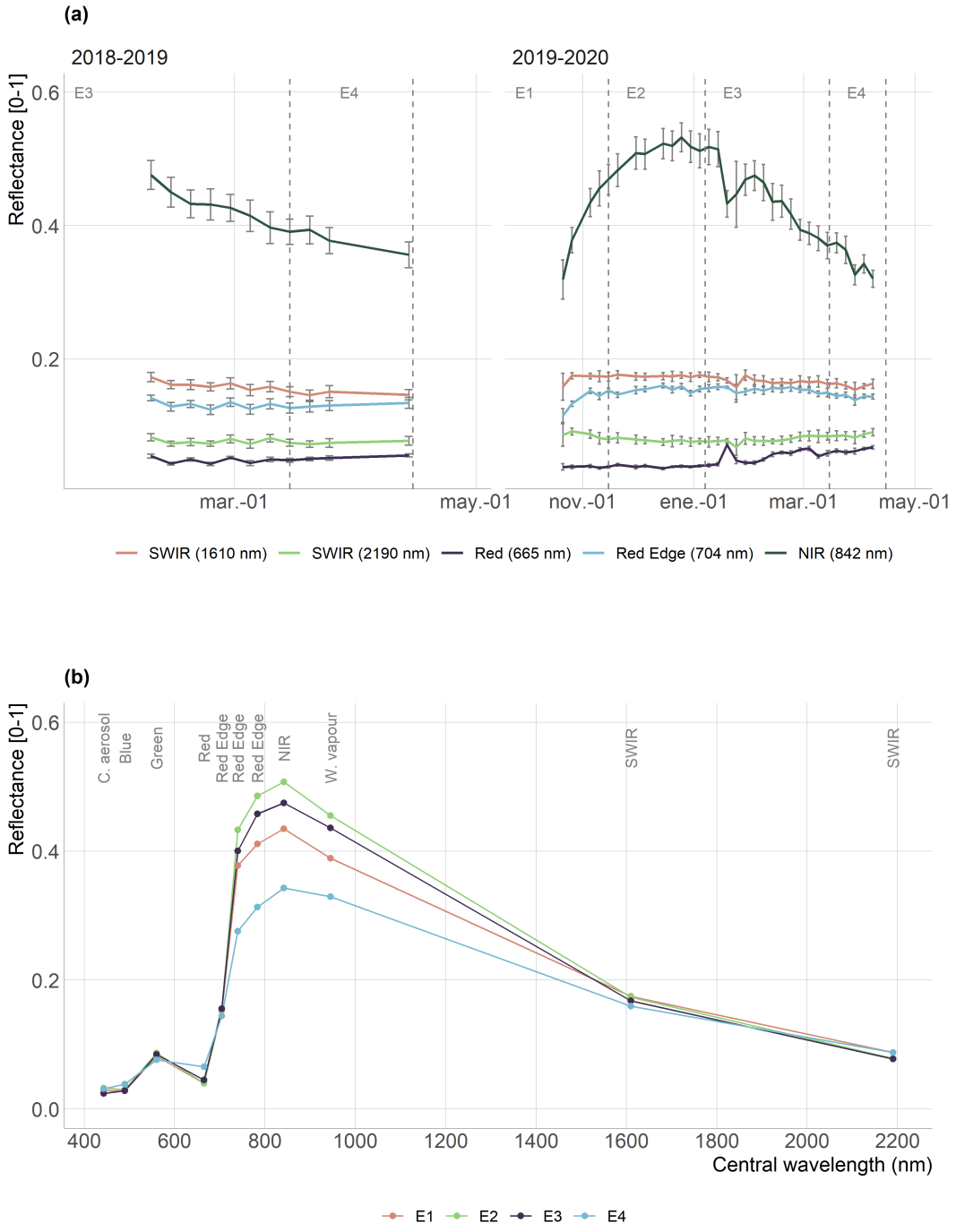

Figure 9. (**a**) Reflectivity of the spectral bands of the vegetation indices. The colored line corresponds to the average of the trees and the vertical lines to the standard deviation. (**b**) Average of the spectral signature of the trees for 2019-11-05 (E1), 2019-12-05 (E2), 2020-02-03 (E3) and 2020-04-03 (E4).

- It was evidenced that the patch pressure (Pp) detected the temporary changes in the hydric state of the leaf, which were attributable both to the phenological behavior of the vegetation and to agricultural management.
- The vegetation indices that obtained the highest relationship with Pp were EVI and Rededge1 for the 2018-2019 and 2019-2020 season, respectively. However, the performance of the vegetation

indices that included the NIR spectral range was influenced by the vegetative development of the crop.

- The Rededge1 index was not sensitive to vegetative development, for which it presented a better performance to monitor the hydric status of the vegetation based on leaf turgor.

We believe that further research could improve by considering conditions where the plant water status is more restricted, considering different irrigation treatments that include plant water stress conditions.

Acknowledgments: This study was financed thanks to the contribution of the FONDECYT project 11190360, of the National Research and Development Agency (ANID), Chile.

Author Contributions: Francisco Zambrano conceive, designed, and performed the experiments; Francisco Zambrano and Alberto Jopia analyzed the data; Waldo Pérez, Paulina Vidal, Julio Molina, and Felipe de la Hoz Mardones contribute with the review of the manuscript and help to make several major improvements.

Conflicts of Interest: The authors declare no conflict of interest. The founding sponsors had no role in the design of the study; in the collection, analyses, or interpretation of data; in the writing of the manuscript, an in the decision to publish the results'.

Abbreviations

The following abbreviations are used in this manuscript:

CARI	Chlorophyll Absorption Ratio IndeX
r^2	Coefficient of determination
EVI	Enhanced Vegetation Index (EVI)
ESA	European Space Agency (ESA)
ET	Evapotranspiration (ET)
GVMI	Global Vegetation Moisture Index (GVMI)
LAI	leaf area index (LAI)
LCI	Leaf Chlorophyll Index (LCI)
NIR	Near infrared (NIR)
NBR	Normalized burn ratio Index (NBR)
NDII	Normalized Difference Infrared Index (NDII)
NDVI	Normalized Difference Vegetation Index (NDVI)
NDWI	Normalized Difference Water Index (NDWI)
Pp	Patch pressure (Pp)
r	Pearson's coefficient
RTM	Radiative transfer model (RTM)
RMSE	Root mean square error (RMSE)
SWIR	Short-wave infrared (SWIR)
SIWSI	Shortwave Infrared Water Stress Index
RDI	Simple Ratio MIR/NIR Ratio Drought Index
SPAC	Soil-plant-atmosphere continuum
ρ	Spearman's non-parametric coefficient rho
BOA	Bottom of the Atmosphere
VNIR	Visible and near infrared
WUE	Water use efficiency

References

1. Misra, A.K. Climate change and challenges of water and food security. *International Journal of Sustainable Built Environment* **2014**, *3*, 153–165. doi:10.1016/j.ijsbe.2014.04.006.
2. Lipper, L.; Thornton, P.; Campbell, B.M.; Baedeker, T.; Braimoh, A.; Bwalya, M.; Caron, P.; Cattaneo, A.; Garrity, D.; Henry, K.; Hottle, R.; Jackson, L.; Jarvis, A.; Kossam, F.; Mann, W.; McCarthy, N.; Meybeck, A.; Neufeldt, H.; Remington, T.; Sen, P.T.; Sessa, R.; Shula, R.; Tibu, A.; Torquebiau, E.F. Climate-smart agriculture for food security. *Nature Climate Change* **2014**, *4*, 1068–1072. doi:10.1038/nclimate2437.
3. Garreaud, R.D.; Alvarez-Garreton, C.; Barichivich, J.; Boisier, J.P.; Christie, D.; Galleguillos, M.; LeQuesne, C.; McPhee, J.; Zambrano-Bigiarini, M. The 2010–2015 megadrought in central Chile: impacts on regional hydroclimate and vegetation. *Hydrology and Earth System Sciences* **2017**, *21*, 6307–6327. doi:10.5194/hess-21-6307-2017.

4. Zambrano, F.; Lillo-Saavedra, M.; Verbist, K.; Lagos, O. Sixteen years of agricultural drought assessment of the biobío region in chile using a 250 m resolution vegetation condition index (VCI). *Remote Sensing* **2016**, *8*, 1–20. doi:10.3390/rs8060530.
5. Zambrano, F.; Wardlow, B.; Tadesse, T.; Lillo-Saavedra, M.; Lagos, O. Evaluating satellite-derived long-term historical precipitation datasets for drought monitoring in Chile. *Atmospheric Research* **2017**, *186*, 26–42. doi:10.1016/j.atmosres.2016.11.006.
6. Zambrano, F.; Vrieling, A.; Nelson, A.; Meroni, M.; Tadesse, T. Prediction of drought-induced reduction of agricultural productivity in Chile from MODIS, rainfall estimates, and climate oscillation indices. *Remote Sensing of Environment* **2018**, *219*, 15–30. doi:10.1016/j.rse.2018.10.006.
7. Boisier, J.P.; Alvarez-Garretón, C.; Cordero, R.R.; Damiani, A.; Gallardo, L.; Garreaud, R.D.; Lambert, F.; Ramallo, C.; Rojas, M.; Rondanelli, R. Anthropogenic drying in central-southern Chile evidenced by long-term observations and climate model simulations. *Elem Sci Anth* **2018**, *6*, 74. doi:10.1525/elementa.328.
8. Zambrano, F.; Molina, M.; Venegas, A.; Molina, J.; Vidal, P. Impact of megadrought on vegetation productivity in Chile: Forest lesser resistant than crops and grassland, 2020.
9. Kirkham, M.B. *Principles of Soil and Plant Water Relations*; Elsevier Inc., 2005. doi:10.1016/B978-0-12-409751-3.X5000-2.
10. Doorenbos, J.; Kassam, A.H. *Yield Response to Water, FAO Irrigation and Drainage Paper 33*; Food and Agriculture Organization of the United Nations: Rome, 1986.
11. Nobel, P.S. *Physicochemical and Environmental Plant Physiology*; Elsevier Inc., 2009. doi:10.1016/B978-0-12-374143-1.X0001-4.
12. Scholander, P.F.; Hammel, H.T.; Bradstreet, E.D.; Hemmingsen, E.A. Sap pressure in vascular plants. *Science* **1965**, *148*, 339–346. doi:10.1126/science.148.3668.339.
13. Ehrenberger, W.; Rüger, S.; Rodríguez-Domínguez, C.M.; Díaz-Espejo, A.; Fernández, J.; Moreno, J.; Zimmermann, D.; Sukhorukov, V.L.; Zimmermann, U. Leaf patch clamp pressure probe measurements on olive leaves in a nearly turgorless state. *Plant Biology* **2012**, *14*, 666–674. doi:10.1111/j.1438-8677.2011.00545.x.
14. Fernández, J.E. Plant-based sensing to monitor water stress: Applicability to commercial orchards. *Agricultural Water Management* **2014**, *142*, 99–109. doi:10.1016/j.agwat.2014.04.017.
15. Rodriguez-Dominguez, C.M.; Hernandez-Santana, V.; Buckley, T.N.; Fernández, J.E.; Diaz-Espejo, A. Sensitivity of olive leaf turgor to air vapour pressure deficit correlates with diurnal maximum stomatal conductance. *Agricultural and Forest Meteorology* **2019**, *272-273*, 156–165. doi:10.1016/j.agrformet.2019.04.006.
16. Westhoff, M.; Schneider, H.; Zimmermann, D.; Mimietz, S.; Stinzing, A.; Wegner, L.; Kaiser, W.; Krohne, G.; Shirley, S.; Jakob, P.; Bamberg, E.; Bentrup, F.W.; Zimmermann, U. The mechanisms of refilling of xylem conduits and bleeding of tall birch during spring. *Plant Biology* **2008**, *10*, 604–623. doi:10.1111/j.1438-8677.2008.00062.x.
17. Zimmermann, U.; Bitter, R.; Marchiori, P.E.R.; Rüger, S.; Ehrenberger, W.; Sukhorukov, V.L.; Schüttler, A.; Ribeiro, R.V. A non-invasive plant-based probe for continuous monitoring of water stress in real time: a new tool for irrigation scheduling and deeper insight into drought and salinity stress physiology. *Theoretical and Experimental Plant Physiology* **2013**, *25*, 2–11. doi:10.1590/s2197-00252013000100002.
18. Beauzamy, L.; Nakayama, N.; Boudaoud, A. Flowers under pressure: Ins and outs of turgor regulation in development, 2014. doi:10.1093/aob/mcu187.
19. Jones, H.G. *Plants and microclimate: A quantitative approach to environmental plant physiology*; Vol. 9780521279, Cambridge University Press, 2013; pp. 1–407. doi:10.1017/CBO9780511845727.
20. Zimmermann, D.; Reuss, R.; Westhoff, M.; Geßner, P.; Bauer, W.; Bamberg, E.; Bentrup, F.W.; Zimmermann, U. A novel, non-invasive, online-monitoring, versatile and easy plant-based probe for measuring leaf water status. *Journal of Experimental Botany* **2008**, *59*, 3157–3167. doi:10.1093/jxb/ern171.
21. Rüger, S.; Ehrenberger, W.; Arend, M.; Geßner, P.; Zimmermann, G.; Zimmerann, D.; Bentrup, F.W.; Nadler, A.; Raveh, E.; Sukhorukv, V.L.; Zimmermann, U. Comparative monitoring of temporal and spatial changes in tree water status using the non-invasive leaf patch clamp pressure probe and the pressure bomb. *Agricultural Water Management* **2010**, *98*, 283–290. doi:10.1016/j.agwat.2010.08.022.

22. Jacquemoud, S.; Ustin, S.L.; Verdebout, J.; Schmuck, G.; Andreoli, G.; Hosgood, B. Estimating leaf biochemistry using the PROSPECT leaf optical properties model. *Remote Sensing of Environment* **1996**, *56*, 194–202. doi:10.1016/0034-4257(95)00238-3.
23. Penuelas, J.; Filella, I.; Biel, C.; Serrano, L.; Save, R. The reflectance at the 950-970 nm region as an indicator of plant water status. *International Journal of Remote Sensing* **1993**, *14*, 1887–1905. doi:10.1080/01431169308954010.
24. Chávez, R.O.; Clevers, J.G.; Herold, M.; Ortiz, M.; Acevedo, E. Modelling the spectral response of the desert tree prosopis tamarugo to water stress. *International Journal of Applied Earth Observation and Geoinformation* **2012**, *21*, 53–65. doi:10.1016/j.jag.2012.08.013.
25. Knapp, A.K.; Carter, G.A. Variability in leaf optical properties among 26 species from a broad range of habitats. *American Journal of Botany* **1998**, *85*, 940–946. doi:10.2307/2446360.
26. Ourcival, J.M.; Joffre, R.; Rambal, S. Exploring the relationships between reflectance and anatomical and biochemical properties in Quercus ilex leaves. *New Phytologist* **1999**, *143*, 351–364. doi:10.1046/j.1469-8137.1999.00456.x.
27. Colombo, R.; Meroni, M.; Marchesi, A.; Busetto, L.; Rossini, M.; Giardino, C.; Panigada, C. Estimation of leaf and canopy water content in poplar plantations by means of hyperspectral indices and inverse modeling. *Remote Sensing of Environment* **2008**, *112*, 1820–1834. doi:10.1016/j.rse.2007.09.005.
28. Bai, T.; Zhang, N.; Mercatoris, B.; Chen, Y. Jujube yield prediction method combining Landsat 8 Vegetation Index and the phenological length. *Computers and Electronics in Agriculture* **2019**, *162*, 1011–1027. doi:10.1016/j.compag.2019.05.035.
29. Karkauskaite, P.; Tagesson, T.; Fensholt, R. Evaluation of the plant phenology index (PPI), NDVI and EVI for start-of-season trend analysis of the Northern Hemisphere boreal zone. *Remote Sensing* **2017**, *9*. doi:10.3390/rs9050485.
30. Raghavendra, B.R.; Mohammed Aslam, M.A. Sensitivity of vegetation indices of MODIS data for the monitoring of rice crops in Raichur district, Karnataka, India. *Egyptian Journal of Remote Sensing and Space Science* **2017**, *20*, 187–195. doi:10.1016/j.ejrs.2016.06.005.
31. Xe, J.; Su, B. Significant remote sensing vegetation indices: A review of developments and applications. *Journal of Sensors* **2017**, *2017*. doi:10.1155/2017/1353691.
32. Rouse, J.W.; Haas, R.H.; Schell, J.A.; Deering, D.W. Monitoring vegetation systems in the Great Plains with ERTS **1973**.
33. Huete, A.; Didan, K.; Miura, H.; Rodriguez, E.; Gao, X.; Ferreira, L. Overview of the radiometric and biopyhsical performance of the MODIS vegetation indices. *Remote Sensing of Environment* **2002**, *83*, 195–213.
34. Gerhards, M.; Schlerf, M.; Rascher, U.; Udelhoven, T.; Juszczak, R.; Alberti, G.; Miglietta, F.; Inoue, Y. Analysis of Airborne Optical and Thermal Imagery for Detection of Water Stress Symptoms. *Remote Sensing* **2018**, *10*, 1139. doi:10.3390/rs10071139.
35. Gerhards, M.; Schlerf, M.; Mallick, K.; Udelhoven, T. Challenges and Future Perspectives of Multi-/Hyperspectral Thermal Infrared Remote Sensing for Crop Water-Stress Detection: A Review. *Remote Sensing* **2019**, *11*, 1240. doi:10.3390/rs11101240.
36. Ji, L.; Zhang, L.; Wylie, B.K.; Rover, J. On the terminology of the spectral vegetation index (NIR - SWIR)/(NIR+SWIR). *International Journal of Remote Sensing* **2011**, *32*, 6901–6909. doi:10.1080/01431161.2010.510811.
37. Kim, D.M.; Zhang, H.; Zhou, H.; Du, T.; Wu, Q.; Mockler, T.C.; Berezin, M.Y. Highly sensitive image-derived indices of water-stressed plants using hyperspectral imaging in SWIR and histogram analysis. *Scientific Reports* **2015**, *5*. doi:10.1038/srep15919.
38. Hardisky, M.A.; Klemas, V.; Smart, R.M. The Influence of Soil Salinity, Growth Form, and Leaf Moisture on the Spectral Radiance of Spartina alterniflora Canopies. *Photogrammetric Engineering and Remote Sensing* **1983**, *49*, 77–83.
39. Gao, B.C. {NDWI-A} normalized difference water index for remote sensing of vegetation liquid water from space. *Remote Sensing of Environment* **1996**, *58(3)*, 257–266.
40. Fensholt, R.; Sandholt, I. Derivation of a shortwave infrared water stress index from MODIS near- and shortwave infrared data in a semiarid environment. *Remote Sensing of Environment* **2003**, *87*, 111–121. doi:10.1016/j.rse.2003.07.002.

41. Xiao, X.; Hollinger, D.; Aber, J.; Goltz, M.; Davidson, E.A.; Zhang, Q.; Moore, B. Satellite-based modeling of gross primary production in an evergreen needleleaf forest. *Remote Sensing of Environment* **2004**, *89*, 519–534. doi:10.1016/j.rse.2003.11.008.
42. ESA. ESA - SENTINEL 2, 2015.
43. Frampton, W.J.; Dash, J.; Watmough, G.; Milton, E.J. Evaluating the capabilities of Sentinel-2 for quantitative estimation of biophysical variables in vegetation. *ISPRS Journal of Photogrammetry and Remote Sensing* **2013**, *82*, 83–92. doi:10.1016/j.isprsjprs.2013.04.007.
44. Beck, H.E.; Zimmermann, N.E.; McVicar, T.R.; Vergopolan, N.; Berg, A.; Wood, E.F. Present and future köppen-geiger climate classification maps at 1-km resolution. *Scientific Data* **2018**, *5*, 1–12. doi:10.1038/sdata.2018.214.
45. DGA. Pronóstico de caudales de deshielo temporada de riego 2019-2020. Technical report, Dirección General de Aguas. Ministerio de Obras Públicas, Gobierno de Chile, Santiago, Chile., 2019.
46. Allen G., R.; Pereira, L.S.; Raes, D.; Smith, M. *Evapotranspiración del cultivo*; 2006; p. 297, [arXiv:1011.1669v3]. doi:10.1016/j.msea.2011.05.042.
47. Sabaini, C.; Goecke, P. Hacia la produccion de un kiwi hayward más homogenéo y dulce. *Fruticola* **2013**, *2*, 17–23.
48. Sabaini, C. Manejo productivo del kiwi orientado a obtener un producto rico y homogéneo. Technical report, Fedefruta, ASOEX, 2012.
49. Ranghetti, L.; Boschetti, M.; Nutini, F.; Busetto, L. "sen2r": An R toolbox for automatically downloading and preprocessing Sentinel-2 satellite data. *Computers and Geosciences* **2020**, *139*. doi:10.1016/j.cageo.2020.104473.
50. R Core Team. R: The R Project for Statistical Computing, 2020.
51. Cloutis, E.A.; Connery, D.R.; Dover, F.J.; Major, D.J. Airborne multi-spectral monitoring of agricultural crop status: Effect of time of year, crop type and crop condition parameter. *International Journal of Remote Sensing* **1996**, *17*, 2579–2601. doi:10.1080/01431169608949094.
52. Datt, B. Remote sensing of water content in Eucalyptus leaves. *Australian Journal of Botany* **1999**, *47*, 909–923. doi:10.1071/BT98042.
53. Kim, M.S.; Daughtry, C.S.T.; Chappelle, E.W.; Mcmurtrey, J.E.; Walthall, C.L. The Use of High Spectral Resolution Bands for Estimating Absorbed Photosynthetically Active Radiation (A Par). Technical report, kim1994, 1994.
54. Key, C.H.; Benson, N.; Ohlen, D.; Howard, S.; McKinley, R.; Zhu, Z. The Normalized Burn Ratio and relationships to burn severity ...; , 2002.
55. Ceccato, P.; Flasse, S.; Grégoire, J.M. Designing a spectral index to estimate vegetation water content from remote sensing data: Part 1: Theoretical approach. *Remote Sensing of Environment* **2002**, *82*, 188–197. doi:10.1016/S0034-4257(02)00037-8.
56. Pinder, J. W, I.; Mcleod, K. Indications of Relative Drought Stress in Longleaf Pine from Thematic Mapper Data. *Photogrammetric Engineering & Remote Sensing* **1999**, *65*, 495–501.
57. Becker, R.A.; Chambers, J.M.; Wilks, A.R. *The new S language: a programming environment for data analysis and graphics* |; Wadsworth and Brooks/Cole Advanced Books & Software: Monterey, CAUnited States, 1988.
58. Pearson, K. Notes on the history of correlation. *Biometrika* **1920**, *13*, 25–45. doi:10.1093/BIOMET.
59. Spearman, C. The proof and measurement of association between two things. *The American journal of psychology* **1904**, *15*, 72–101. doi:10.2307/1422689.
60. Hahn, G.J. The Coefficient of Determination Exposed. *Chemical Technology* **1973**, *3*, 609–612.
61. Wilks, D.S. *Statistical Methods in the Atmospheric Sciences*, second ed.; 2006; p. 649.
62. Keller, M. *Phenology and growth cycle*; 2020; pp. 61–103. doi:10.1016/b978-0-12-816365-8.00002-6.
63. Jensen, J.R. *Remote sensing of the environment: an earth resource perspective second edition*; Vol. 1, 2014; pp. 333–378.
64. Ollinger, S.V.; Richardson, A.D.; Martin, M.E.; Hollinger, D.Y.; Frolking, S.E.; Reich, P.B.; Plourde, L.C.; Katul, G.G.; Munger, J.W.; Oren, R.; Smith, M.L.; Paw U, K.T.; Bolsta, P.V.; Cook, B.D.; Day, M.C.; Martin, T.A.; Monson, R.K.; Schmid, H.P. Canopy nitrogen, carbon assimilation, and albedo in temperate and boreal forests: Functional relations and potential climate feedbacks. *Proceedings of the National Academy of Sciences of the United States of America* **2008**, *105*, 19336–19341. doi:10.1073/pnas.0810021105.

65. Soria-Ruiz, J.; Fernandez-Ordonez, Y.; McNair, H. Corn Monitoring and Crop Yield Using Optical and Microwave Remote Sensing. *Geoscience and Remote Sensing* **2009**. doi:10.5772/8311.
66. Vreugdenhil, M.; Wagner, W.; Bauer-Marschallinger, B.; Pfeil, I.; Teubner, I.; Rüdiger, C.; Strauss, P. Sensitivity of Sentinel-1 backscatter to vegetation dynamics: An Austrian case study. *Remote Sensing* **2018**, *10*, 1–19. doi:10.3390/rs10091396.
67. Ihuoma, S.O.; Madramootoo, C.A. Recent advances in crop water stress detection, 2017. doi:10.1016/j.compag.2017.07.026.
68. Moran, M.S.; T.R., C.; Inoue, Y.; Vidal, A. Estimating crop water defficiency using the relation between surface minus air temperature and spectral vegetation index. *Remote Sens. Environ.* **1994**, *49*, 246–263. doi:10.1016/0034-4257(94)90020-5.
69. Vicente-Serrano, S.M.; Pons-Fernández, X.; Cuadrat-Prats, J.M. Mapping soil moisture in the central Ebro river valley (northeast Spain) with Landsat and NOAA satellite imagery: A comparison with meteorological data. *International Journal of Remote Sensing* **2004**, *25*, 4325–4350. doi:10.1080/01431160410001712990.
70. Wang, K.; Li, Z.; Cribb, M. Estimation of evaporative fraction from a combination of day and night land surface temperatures and NDVI: A new method to determine the Priestley-Taylor parameter. *Remote Sensing of Environment* **2006**, *102*, 293–305. doi:10.1016/j.rse.2006.02.007.